Backscattering Cross Sections for Ionization of Surface-Atom K Shells by Electron Impact*

Robert L. Gerlach and A. R. DuCharme
Sandia Laboratories, Albuquerque, New Mexico 87115
(Received 28 December 1972)

Backscattering cross sections for the electron-impact K-shell ionization of C, N, O, Na, and Mg adsorbed on a tungsten (100) surface are reported. The ionization event studied is the scattering of K-shell electrons to unfilled states within a few eV of the Fermi level of the W substrate. These data are obtained through a new technique which analyzes the currents in ionization-loss features by comparing them with the currents in the elastic peaks. This technique involves numerical simulation of the ionization features using distribution functions. Measured cross sections in the backscattered region are compared with the Burhop theory over an energy range extending from one to four times the ionization energy. The measured and calculated cross sections decrease with increased atomic number and with primary energy. Although some improvement in shape agreement is noted with increased atomic number, the experimentally derived backscattering cross sections exceed the calculated values for the entire energy range investigated. It is shown that the disagreement noted, even for the higher-energy range studied, cannot be attributed to double-scattering processes. The simple theory based on the first Born approximation, although reasonable in total-cross-section determination, is not accurate enough to account for behavior in the backscattered region.

I. INTRODUCTION

One important aspect to the study of inner-shell ionization by electron impact is the obtaining of cross-section information, usually expressed as a function of primary-electron energy. A considerable amount of experimental effort has been devoted to the measurement of total cross sections[1-7] for the K-shell ionization of atoms. Such measurements are important to the evaluation of existing electron-atomic collision theory and to the continued development of ionization, Auger, and x-ray spectroscopies.

The principal method for obtaining total cross sections for K-shell ionization of atoms by electron impact is the measurement[1-6,8-10] of the efficiency of excitation of characteristic x radiation. In this procedure, intensities of x-ray lines resulting from the filling of K-shell vacancies are determined. Total cross sections obtained by this approach include those for the K-shell ionization of Ag by Clark[1]; of Ni by Smick and Kirkpatrick[2]; of Cu, Ag, and Ni by Green[3]; of Sn and Au by Motz and Placious[4]; of Zr, Sn, and W by Hansen *et al.*[5]; and of Al by Hink and Ziegler.[6]

Complementing the x-ray technique for low-Z targets (where the fluorescent yields are small) is the determination of total cross sections via the Auger spectrum. Here the determination of Auger electron intensities can lead to total-cross-section determinations. This approach was used by Glupe and Mehlhorn[7] to measure total cross sections for the K-shell ionization of C, N, O, and Ne.

Until recently, differential cross sections for the K-shell ionization of atoms by electron impact have been obtained only for very light elements in gaseous form. Angular selection of the inelastically scattered electron intensity is typically made by means of a slit system. This technique was used by Mohr and Nicoll[11] to obtain the differential cross section for the ionization of He. Their results illustrate the rapid decrease in ionization cross section with scattering angle at high energies.

A theory based on the first Born approximation was derived by Burhop[12] and extended by Arthurs and Moiseiwitsch[13] to describe the K-shell ionization of isolated atoms by electron impact. Burhop, comparing calculations derived from his theory with experimental total cross sections for the K-shell ionization of Ni and Ag, found good agreement even for rather low energies. More recently, other total-cross-section tests of the theory have been performed.[6,7] However, Massey and Burhop[14] demonstrated the inadequacy of the first-Born-approximation treatment of backscattering in the ionization of He. The theory is shown to decrease much too rapidly with increasing scattering angle. A test of the theoretical approximations for backscattering has not been made for heavier elements, however, due to the lack of angularly dependent data.

In a recent paper[15] we presented a new method for backscattering cross-section determination of K-shell ionization of atoms adsorbed on a metal surface. In this approach, inelastically scattered primary electrons are detected in the weak 128° to 148° backscattering region. Cross-section data for C, N, and O were compared with the Burhop

theory.

The secondary-electron energy distribution resulting from electron impact of a solid surface contains fine structure of two general types. Fixed-energy fine structure, such as Auger peaks, and fixed-loss-energy structure, such as ionization steps, [16-18] appear in the energy distribution. It has been shown[7] that Auger peaks can provide a determination of the electron-induced total ionization cross sections of the core levels of atoms. In this paper we show that the ionization fine structure provides cross sections which can be studied over small ranges in energy and angle. We extend our improved measurement capability to Mg and Na and compare with the Burhop theory.

The ionization process is depicted by the energy-level diagram in Fig. 1. An electron with primary energy E_p incident on a solid surface scatters a core electron with binding energy E_k to an unfilled energy state with energy ϵ above the Fermi level. [15,16] The scattered primary electron has lost energy $E_L = E_k + \epsilon$ by the encounter (exchange is neglected in this simple description). Since the minimum loss energy for this ionization process is E_k, a step appears in the secondary-electron energy distribution with its edge E_k eV below the elastic peak. By observing the number of backscattered electrons within 3 eV of the edge of the ionization step, a class of ionization cross sections may be determined. These cross sections closely resemble those for excitation since they are for fixed loss energy. They are integrated over a 128° to 148° backscattering angle and a small range of ejected-electron energy.

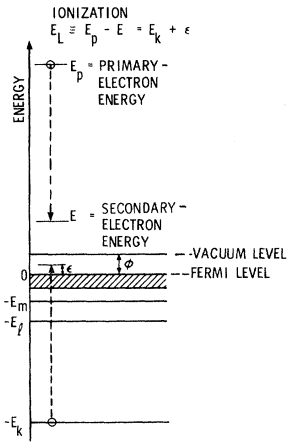

FIG. 1. Energy-level diagram of a metal surface depicting the electron-impact ionization of an inner shell of an atom. The energies E_m, E_1, and E_k are electron binding or ionization energies of inner shells of surface atoms. E_L is the loss energy.

II. TECHNIQUES AND APPARATUS

The apparatus for measurement of backscattering ionization cross sections of surface atoms is shown in Fig. 2. It is composed of an electron gun, a two-stage electron energy analyzer, and electronics for differentiation of the energy distribution by synchronous detection. Constant-loss-energy structure in the energy distribution is observed by sweeping the electron-gun energy while maintaining a constant bandpass energy with the electron energy analyzer. [18] The loss-energy fine structure is accentuated with respect to the slowly varying background by double differentiation with respect to secondary-electron energy. This differentiation is accomplished by applying a sinusoidal voltage to the outer cylinder of the cylindrical mirror analyzer and detecting the second-harmonic current signal with the tuned tank and phase-lock amplifier. [18,19]

The electron gun is composed of a Pierce gun[20] with a 0.15-cm-wide W filament followed by an electrostatic lens. The gun is capable of emitting 1 mA at 1000-eV energy in a 0.25-cm-diam spot size. Currents of 25 to 500 μA are employed in the cross-section measurements. Constant electron current from the gun is maintained by a feedback circuit. The energy width of the electron beam is less than 1 eV.

The retarding analyzer is composed of 40-lines/cm W wire-mesh spherical segments of 2.15- and 2.40-cm radii. The cylindrical mirror analyzer[21-23] has an inner cylinder radius of 2.54 cm and 10° half-angle apertures. Helmholtz coils are employed to reduce the static magnetic field to about 30 mG in the region of the analyzer. The design resolution of the cylindrical analyzer is 2%, but electron beam size and residual magnetic fields increase this to 3%. It may be noted that the analyzer bandpass energy is the sum of the retarding energy plus the cylindrical analyzer bandpass energy. The combined retarding-field cylindrical mirror analyzer has better than 2-eV resolution for 0 to 1500 eV, but a resolution of 3 eV was commonly employed with the bandpass energy of the cylindrical analyzer at 90 eV. This absolute resolution is constant to within about 50% over the energy range employed.

The transmission of the analyzer, for electrons backscattered into the aperture between 128° and 148°, was determined experimentally. With the sample and first retarding grid fixed at +500 V, a retarding-field plot was obtained by varying the gun potential from about +10 to −10 V. The secondary-electron current incident on the 20°-wide analyzer aperture was equal to the sum of the electron-gun current, target current, and first-grid aperture current after correction for absorption by the first retarding grid wires. The elastic current, ob-

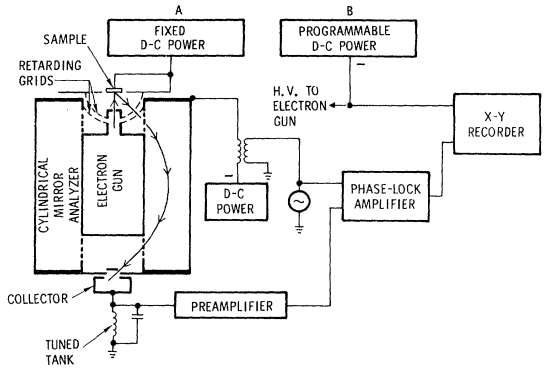

FIG. 2. Simplified schematic of apparatus employed to measure backscattering cross sections. Loss energy or ionization spectra are obtained with power supply B programed for voltage sweep and with second-harmonic detection of the energy-analyzed current. The outer retarding grid and inner analyzer cylinder are at ground potential.

tained from the retarding plot, was divided into the peak-analyzed elastic current (collected at the end of the analyzer) to obtain the transmission factor T. The transmission determined from this procedure is 0.083 ± 0.02 for 500-V retarding potential and no bias on the collector. The above procedure was repeated at other retarding voltages to determine the change of transmission with retarding energy. The transmission was observed to decrease to about 0.05 at 1500-V retarding potential.

Synchronous detection was performed at 8 kHz, which is twice the fundamental frequency applied to the analyzer cylinder. A 1.5-V rms potential was applied to the outer analyzer cylinder in order to oscillate the bandpass energy 2.0 eV rms. A tuned L-C tank of (4×10^7)-Ω impedance at 8 kHz allowed detection of total analyzed current down to 10^{-8} A before thermal noise dominated over shot noise. With 10^{-8}-A total analyzed current, signals as low as 10^{-14} A could be detected, allowing for integration of shot noise over periods of about 1 sec by the phase-lock amplifier.

The measurements were performed in a bakeable ultrahigh vacuum system. Operating pressures were 10^{-10}–10^{-9} Torr. The W(100) substrate was cleaned by heating in O_2 and then in vacuum.[24] Oxygen, nitrogen, and carbon (in the form of ethylene) were admitted to pressures of about 10^{-6} Torr for approximately 1 min to assure near saturation on the W(100) surface at about 100 °C. Sodium was evaporated from a Pyrex ampoule[25] and Mg from a W wire. Purity of the deposits was verified by Auger[23] and ionization[18] spectroscopy; impurities were usually kept below $\frac{1}{10}$ monolayer, though they generally affected the measurements only slightly. Cross-section measurements at an arbitrary energy were periodically repeated during a run to check for reduced coverage of the adsorbed species by possible electron-beam-induced desorption, beam heating, or displacement by background gases. Only nitrogen was found to decay appreciably with time. Therefore, the nitrogen measurements were performed as rapidly as possible and corrections were made for the time-dependent reduction of N on the surface.

III. IONIZATION SPECTRA AND CROSS-SECTION MEASUREMENTS

An elastic peak and ionization spectra for C (ethylene), N, O, Na, and Mg adsorbed on W(100) are shown in Fig. 3. The negative double derivative of the energy distribution with respect to secondary-electron energy $\partial^2 N(E, E_p)/\partial E^2$, at fixed secondary-electron energy E_0, is plotted as a function of loss energy E_L. The zero of the loss-energy scale is defined at the first minimum of the elastic feature and the energy of any ionization feature is measured at its first minimum.[18] The agreement of observed and electron spectroscopy for chemical-analysis[26] electron binding energies is within 2 eV, which is approximately the maximum expected chemical energy shift for C, N, O, Na, or Mg chemically combined with a transition

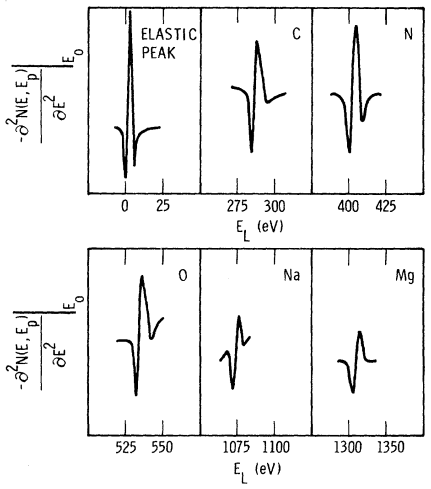

FIG. 3. Double-differentiated elastic peak and K-shell ionization spectra for various elements adsorbed independently on W(100). Loss energy E_L is arbitrarily measured with respect to the low-loss-energy minimum of the elastic peak. The primary energy and gain used to obtain each curve are different; the relative magnitudes of the ionization peaks are contained in Fig. 5. A 3.0-eV analyzer resolution and 2.0-eV rms bandpass oscillation amplitude were employed for all spectra except Mg; for Mg 6-eV analyzer resolution and 4.0-eV rms bandpass oscillation amplitude were used. Note the compressed energy scale for Mg.

metal.[26,27] The shapes of the spectra were shown to be independent of primary energy, within experimental error. A model will now be developed to determine how these ionization spectra may yield backscattering ionization cross sections.

Simulated electron-energy-analyzer detection and electronic double differentiation of a peak and of a step are shown in Fig. 4. For this simulation, the instrument response is closely approximated by the function $G(E)$:

$$G(E) = T\phi(E/W)\,, \tag{3.1}$$

where $\phi(\epsilon)$ is given by

$$\phi(\epsilon) = [1/(2\pi)^{1/2}]\, e^{-\epsilon^2/2}\,,$$

T is the analyzer transmission, and $2W$ is the instrument response width. The energy spread of the primary electron beam and analyzer resolution are both contained in W. Let the true elastic peak and ionization step be given by the distribution functions

$$N_p(E_L) = I_p\,\delta(E_L - E_p) \quad \text{(peak)} \tag{3.2a}$$

and

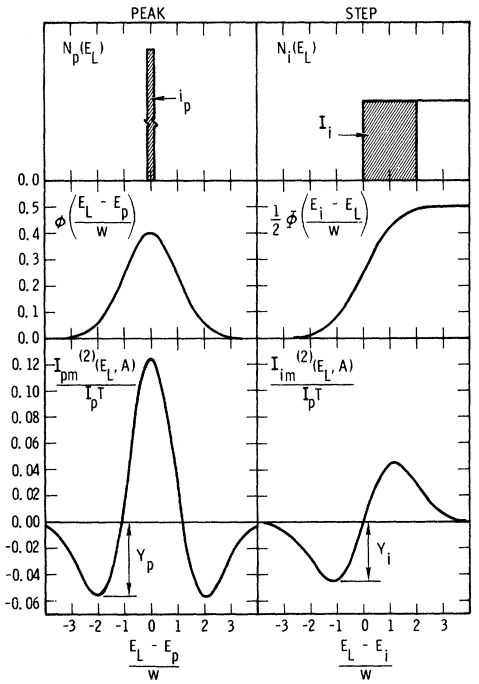

FIG. 4. Numerical simulation of the second-harmonic synchronous detection of an elastic peak and an ionization step. The current distributions N_p and N_i are convoluted with the normally distributed instrument response giving the measured currents I_{pm} and I_{im}. Second-harmonic synchronous detection produces the double derivatives $I_{pm}^{(2)}$ and $I_{im}^{(2)}$. The shapes of $I_{pm}^{(2)}$ and $I_{im}^{(2)}$ are to be compared with the corresponding experimental ones in Fig. 3.

$$N_i(E_L) = (I_i/2W)\int_0^{E_L} \delta(E' - E_i)\, dE' \quad \text{(step)}\,, \tag{3.2b}$$

where $\delta(E)$ is the Dirac δ function; E_p and E_i are primary-electron and ionization step energy, respectively; and I_p is the current in the (elastic) peak. We want the current I_i contained within energy $2W$ of the ionization step edge as depicted in Fig. 4.

The measured analyzer current is the convolution of the true peak or step-current distribution with the instrument response:

$$\begin{aligned} I_{pm}(E_L) &= N_p(E_L) * G(E_L) \\ &= \int_{-\infty}^{\infty} N_p(E')\, G(E_L - E')\, dE' \\ &= I_p\, T\, \phi[(E_L - E_p)/W] \end{aligned} \tag{3.3a}$$

and

$$\begin{aligned} I_{im}(E_L) &= (I_i/2W)\int_{E_i}^{\infty} G(E_L - E')\, dE' \\ &= \tfrac{1}{2}(I_i\, T)\,\Phi[(E_i - E_I)/W]\,, \end{aligned} \tag{3.3b}$$

where

$$\Phi(\epsilon) = [1/(2\pi)^{1/2}]\int_{-\infty}^{\epsilon} e^{-x^2/2}\, dX\,,$$

the normal distribution function. The functions (3.3a) and (3.3b) are shown in Fig. 4.

Second-harmonic synchronous detection obtains the second Fourier coefficient of the measured current as a function of loss energy. The bandpass energy of the analyzer is modulated by $-A\sin\omega t$. Since $E_L = E_p - E$, where E_p is not varied, this is equivalent to oscillating the loss energy by $+A\sin\omega t$. Thus, the second-harmonic current signal is[28]

$$I_m^{(2)}(E_L, A) = (1/\pi)\int_0^{2\pi} I_m(E_L + A\sin\omega t) \times \cos 2\omega t\, d(\omega t)\,, \tag{3.4}$$

where I_m is either I_{pm} or I_{im}, the measured peak or step current. For small oscillations A with respect to the widths of features being observed, this second-harmonic signal is proportional to the second derivative of the current with respect to loss energy[28]:

$$I_m^{(2)}(E_L, A) \propto \frac{-\partial^2}{\partial E_L^2}\, I_m(E_L)\,, \tag{3.5a}$$

or, since $E_L = E_p - E$,

$$I_m^{(2)}(E_L, A) \propto \frac{-\partial^2}{\partial E^2}\, I_m(E_L)\,. \tag{3.5b}$$

For the large oscillation amplitudes A employed here, the derivative peaks are slightly broadened in energy.

Second-harmonic detection of the measured peak and step [(3.3a) and (3.3b)] obtains

$$I_{pm}^{(2)}(E_L, A) = \frac{I_p\, T}{\pi}\int_0^{2\pi} \phi\left(\frac{E_L - E_p + A\sin\omega t}{W}\right)$$

$$\times \cos 2\omega t \, d(\omega t) \quad (3.6a)$$

and

$$I_{im}^{(2)}(E_L, A) = \frac{I_i T}{\pi} \int_0^{2\pi} \tfrac{1}{2} \Phi \left(\frac{E_S - E_L - A \sin\omega t}{W} \right) \times \cos 2\omega t \, d(\omega t) , \quad (3.6b)$$

using (3.4). Numerical simulation of this "double differentiation" is shown in Fig. 4 which was computed for $A/W = 2$. Although the second-harmonic detection gives a distorted derivative, broadened about 10%, for simplicity we will henceforth call it a second derivative. Note the close similarity of the simulated differentiated peak and step in Fig. 4 with the measured ones in Fig. 3. From (3.6a) and (3.6b) it is clear that

$$I_i / I_p = \beta (Y_i / Y_p) , \quad (3.7)$$

where β is a constant determined from the numerical simulations and Y is the amplitude shown in Fig. 4.

At this point we must question one assumption made in this simulation. The true ionization steps are slightly broadened rather than being step functions. This natural broadening, which is less than the instrument response width, widens the measured peaks slightly. The effects of this broadening were computer simulated to obtain the constant β in (3.7) required to interpret the measurements. For the elastic peak, $A/W = 1.3\sqrt{2}$ was employed. For the ionization steps, A/W ranged from $1.3\sqrt{2}$ to $\sqrt{2}$ for the various elements studied, depending on the width of the observed ionization feature. The corresponding β values determined from evaluation of (3.6) for various A/W values are from 1.2 to 1.7.

If I_p and Y_p are measured for an arbitrary elastic peak, the ionization step current I_i may be easily computed from (3.7) after measuring the ionization step-differentiated intensity Y_i. Knowing also the primary-electron current I_0 and the density of adatoms n adsorbed on the W(100) surface, the backscattering ionization cross section is computed from

$$\Delta\sigma = (1/n)(I_i / I_0) , \quad (3.8)$$

where I_i is the ionization step current computed from the experimental data (corrected for analyzer transmission) and the step model described above.

The saturated coverages of C, O, and Na were assumed to be one monolayer[24,25] ($n = 10^{15}$ atoms/cm^2) on W(100) at about 100 °C. Nitrogen coverage was assumed to be $\frac{1}{2}$ monolayer.[29] Magnesium was estimated to form one monolayer when the intensity of its KLL Auger peak was $\frac{1}{4}$ the intensity for many layers of Mg.[30] The coverages for N, O, and Na are believed to be within +10% and −30% of the stated values; the uncertainty of the C and Mg coverages is probably ±50%. The total uncertainties in the measured cross sections average about a factor of 2. This total uncertainty arises from errors in determining analyzer transmission and overlayer coverage and from errors in the use of the ionization step model.

Simulation of the effects of transmission and resolution changes on the measured cross sections show that the shapes of the cross section versus energy curves to be seen in Sec. IV are accurate to within 50% from the low-energy to high-energy limits. If anything, the high-energy cross sections are too low since the analyzer transmission drops and the resolution decreases with increasing energy.

IV. COMPARISON OF MEASURED CROSS SECTIONS WITH THEORY

Measured backscattering K-shell ionization cross sections are shown as dots and solid lines in Fig. 5. The improved calibration procedures have changed the absolute values for C, N, and O slightly from those reported in a previous paper.[15] The peak-to-peak amplitudes of the ionization features of Fig. 3 were measured as a function of reduced primary energy $X \equiv E_p / E_i$, where E_i is the ionization energy (E_k, E_l, ··· in Fig. 1). The procedures described in Sec. III were used to compute the absolute cross sections, with an energy spread of 3 eV and backscattering acceptance angles of 128°–148° being employed in the experiments. This energy spread (energy response width) $2W$ = 3 eV was chosen for two reasons. First of all, higher resolution produced an insufficient signal-to-noise ratio for O and Na. Second, the natural broadening of the ionization steps (~1 eV) must be less than the instrument response width in order for the step model of Sec. III to be valid. (A correction factor for the larger instrument energy bandpass and oscillation amplitude employed for Mg was applied for its cross-section determination.) The carbon measurements were performed both with adsorbed ethylene and with decomposed ethylene (heated to ~1000 °C). No difference in the shape of the cross section versus energy curve was detected for the two states of carbon.

All cross sections decrease monotonically with reduced energy over the energy range studied. The curves become steeper with atomic number. In addition, the absolute cross sections for a given reduced energy decrease rapidly with atomic number.

A first Born approximation theory for ionization of K shells of isolated atoms was formulated by Burhop.[12,13] This theory uses a plane-wave description of the incident electron and a spherical wave for the scattered electron. The initial and final states of the K-shell electron are represented, respectively, by a hydrogenic wave function and a Coulomb wave function. Since the principal contri-

bution to the matrix elements determining the cross section comes from the neighborhood of the K shell, the use of hydrogenic wave functions seems highly satisfactory. The theory has, in fact, given reasonable agreement[6,7,12] with measured total cross sections available for a few elements. The cross-section data we present in this paper may be compared with the Burhop theory for the purpose of obtaining qualitative understanding of the results.

The following expression is found from the Burhop theory for the differential cross sections for K-shell ionization:

$$I(K,\kappa)\,dK\,d\kappa = \frac{2^{11}\pi\mu^6\kappa[K^2+\frac{1}{3}(\mu^2+\kappa^2)][\mu^4+2\mu^2(K^2+\kappa^2)+(K^2-\kappa^2)^2]^{-3}}{a_0^2 k^2 K(1-e^{-2\pi\mu/K})} \times \exp\left[-\frac{2\mu}{\kappa}\arctan\left(\frac{2\mu K}{K^2-\kappa^2+\mu^2}\right)\right]dK\,d\kappa\,, \quad (4.1)$$

where $\mu = Z/a_0$ with a_0 as the Bohr radius. The initial and final momenta of the incident electron, k and k', are related to the momentum of the ejected electron κ and the ionization energy E_i by the energy equation

$$(\hbar^2/2m)(k^2-k'^2) = E_i + \hbar^2\kappa^2/2m\,. \quad (4.2)$$

In order to compare with backscattering experimental data we used the momentum-transfer definition to obtain the angular dependence:

$$K = |\vec{k}-\vec{k}'| = (k^2+k'^2-2kk'\cos\theta)^{1/2}\,, \quad (4.3)$$

where θ is the angle between $\vec{k}$ and $\vec{k}'$. To compare with experimental results, (4.1) must be integrated over κ and θ. According to the step model of Sec. III, the analyzer resolution restricts the upper limit of the integration on the momentum of the ejected electron to conform with an energy spread of 3 eV above the Fermi level (7.5 eV) of the W substrate. The 128° to 148° backscattering accepted by the analyzer defines the limits of integration on θ.

Computed cross sections $\Delta\sigma$ for K-shell ionization of C, N, O, Na, and Mg are shown in Fig. 5 (dashed lines) where they are compared with the corresponding measurements as a function of reduced primary energy. The calculations show the general trend toward reduced cross section with primary energy and atomic number, evidenced by the data, but are considerably lower than the measurements over the entire energy range investigated. Although shape agreement between theory and experiment improves with atomic number, disagreement in absolute magnitudes becomes more pronounced with increased primary energy.

This comparison with theory in the backscattered region is in sharp disagreement with total cross-section[6,7,12] comparisons between first-Born-approximation theory and experiments. These backscattering measurements show that the theory has too strong an energy dependence in the higher-energy regime.

V. DISCUSSION

Double scattering involving elastic reflection by the W(100) substrate plus forward ionization scattering by the overlayer, or *vice versa*, must be considered as a possible explanation for the differences between the experimental cross sections and the single-event theory. Equations for this double scattering are derived in the Appendix and computed double scattering is shown in Fig. 6 for comparison with measured C and Mg cross sections. If the ionization scattering is strongly peaked in the forward direction and the elastic reflectivity of the substrate is a rather smooth function of angle, then the double scattering is accurately described by

$$\Delta\sigma_{ds}(E_p) \approx \rho\Delta\sigma_{fs}(E_p)[R_A(E_p)+R_A(E_p-E_i)]\,, \quad (5.1)$$

where

$$\Delta\sigma_{fs}(E_p) = \int_F \sigma(E_p,\hat{k},\hat{k}')\,d\Omega'\,, \quad (5.2)$$

R_A is the ratio of the elastic current accepted by the analyzer aperture divided by the primary current, and ρ is the absorption factor for the overlayer. The F on the integral in (5.2) indicates that the integration over Ω', the solid angle for the scattered momentum vector $\hat{k}'$, is carried out in the forward direction. For our calculations, the integration was for 0° to 20° between incident and scattered momentum vectors $\hat{k}$ and $\hat{k}'$.

Results of calculations of ionization scattering from the Burhop theory for carbon are shown in Fig. 7 for various scattering angles. The theory demonstrates that forward scattering (0° to 20°) dominates for $X > 2$. (The experimental cross sections indicate that $\Delta\sigma$ may not be so strongly peaked in the forward direction.) In addition, low-energy-electron-diffraction (LEED) measurements show no gross concentrations of elastic intensity over the scattering angles of the analyzer aperture. (Diffraction peaks do not contain much intensity when compared with the surrounding diffuse background.) Thus (5.1) is a good estimate

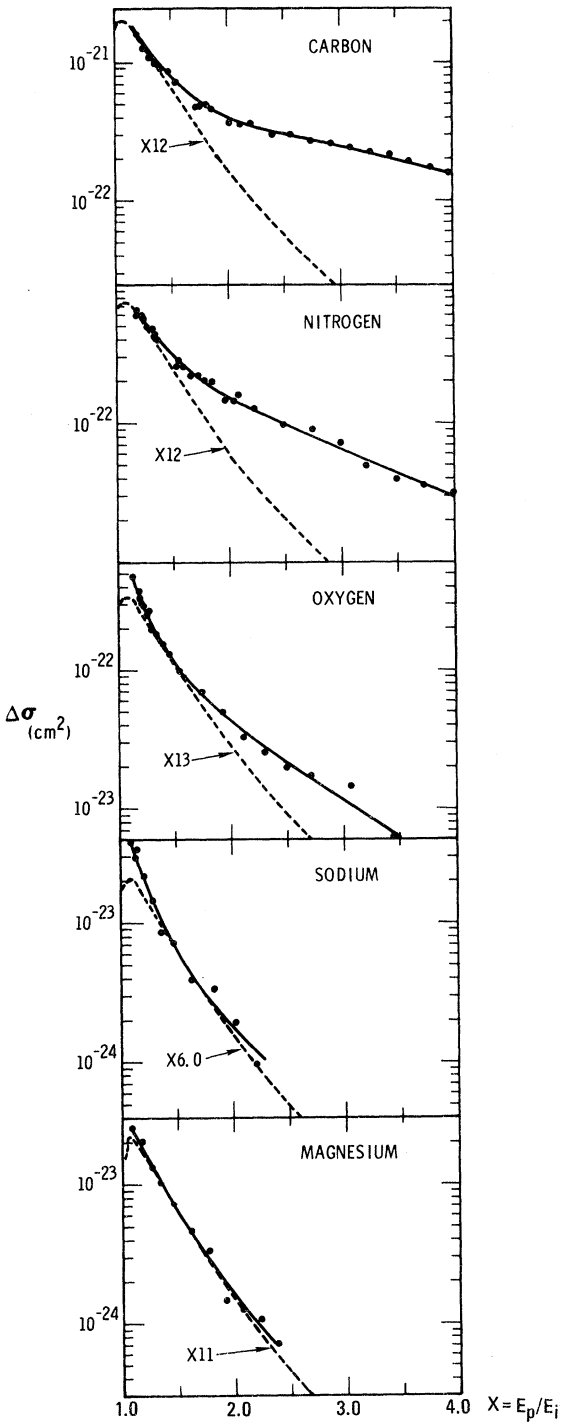

FIG. 5. Backscattering cross sections $\Delta\sigma$ for K-shell ionization of C, N, O, Na, and Mg adsorbed on W(100). These cross sections are for 128° to 148° backscattering angle and ejected electron energy spread of 3 eV. The solid lines are fits of the experimental points. The dotted lines are cross sections computed from the Burhop first-Born-approximation theory for K-shell ionization. These theoretical curves are magnified, as indicated, to be tangent to the experimental curves. The uncertainty in the measured cross sections is a factor of 2.

of double scattering for $X > 2$.

The elastic-reflection coefficient R_A was determined by measuring the elastic-reflection electron current (corrected for transmission) as a function of energy and dividing by the primary-electron current. Results are shown in Fig. 8. These data plus the $\Delta\sigma_{ts}$ calculated from the Burhop theory[12,13] were inserted into (5.1) to estimate the double scattering and are shown as squares in Fig. 7. A value of 0.75 was used for ρ corresponding to the average experimental value for electrons adsorbed by the overlayer. This estimate of double scattering is considered to be accurate within a factor of 2 except for $X < 1.5$. Note that the double scattering computed from (5.1) is at least an order of magnitude below the measured cross section.

At very low energies nearer the ionization threshold, the ionization scattering is more nearly isotropic (see Fig. 7). Assuming that both the elastic and ionization scattering are isotropic, the following equation was derived in the Appendix for double scattering:

$$\Delta\sigma_{ds}(E_p) \approx \rho\sigma_T(E_p)\left[R_A(E_p) + R_A(E_p - E_i)\right], \quad (5.3)$$

where

$$\sigma_T(E_p) = \int_{4\pi} \sigma(E_p, \hat{k}, \hat{k}')\, d\Omega' . \quad (5.4)$$

This estimate of double scattering is shown as triangles in Fig. 6. Equation (5.3) is considered to be an overestimate of double scattering except for X near 1.0. Double scattering thus does not account for the major differences between the single-event ionization theory and experiment.

One must consider that all cross sections computed from the Burhop equation might be too small, making the computed double scattering too small. However, the Burhop theory produces reasonable total cross sections (integrated over angle and energy) for K-shell ionization of C, N, and O.[7] These and other comparisons[6,7,12] support the validity of the Burhop theory for small scattering angles. Thus we believe that the computed double scattering is as accurate as stated. Alternatively, one might consider that our measured absolute cross sections are too high. However, measurements[31] of total cross sections using the same apparatus and surfaces agree with the Glupe–Mehlhorn[7] measurements within a factor of 2. Within these considerations, our measured cross sections are as accurate as stated.

Since the ejected electrons in our investigation occupy low-energy states, one might presume that the Burhop theory, which is an atomic formulation, must be altered to include substrate band-structure effects as well as effects of the local chemical environment of the ionized atom. We assume in our application of the Burhop theory to surfaces that the ejected electrons occupy empty

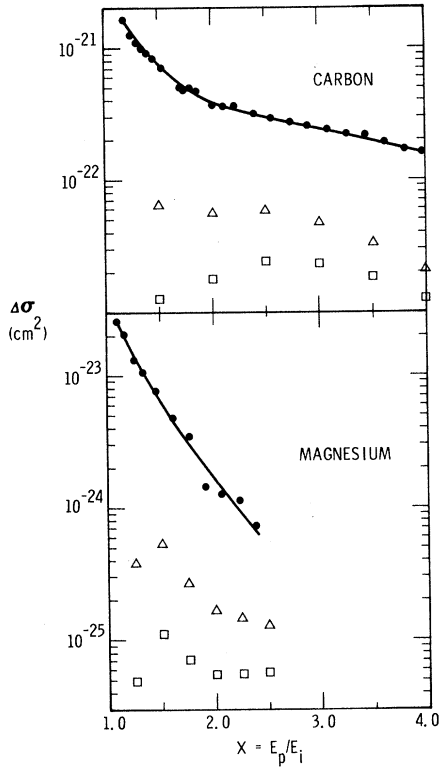

FIG. 6. Double scattering, involving ionization by the overlayer and backward elastic scattering by the substrate, in comparison with the experimental ionization cross sections for C and Mg (solid lines). The double scattering was computed from Eqs. (5.1) and (5.3) giving the squares and triangles, respectively. The squares are considered to be the better estimate of double scattering over all but the lowest part of the energy range.

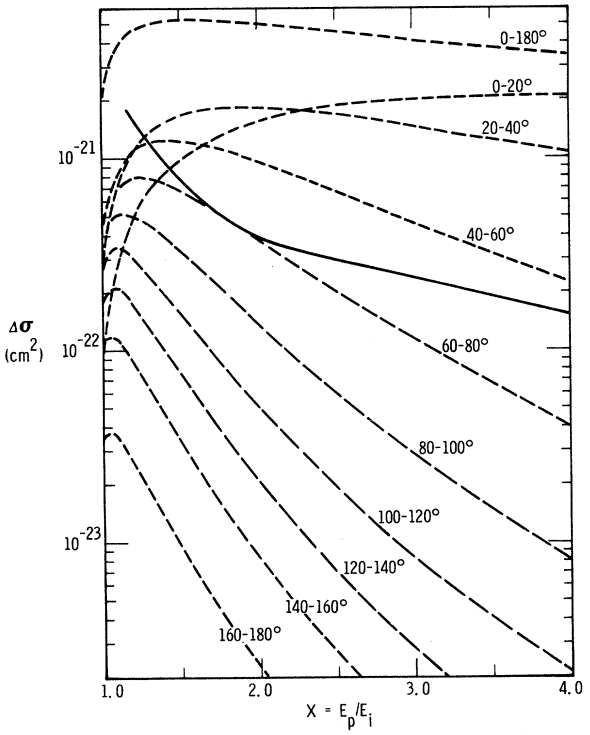

FIG. 7. Ionization scattering for C(K) calculated from the Burhop theory for various scattering angles θ, measured from the forward direction (dotted lines), compared with experimental data for carbon K-shell ionization (solid line), measured for 128°–148° backscattering angles.

states above the Fermi level of the substrate and are free electron in energy behavior. We do this by integrating from the conduction-band depth (7.5 eV for W)[32] to 3 eV above the Fermi level and assume the energy behavior of the ejected electron $E(\kappa)$ to be determined by (4.2).

In the calculations of the backscattering cross section, (4.1) was found to be a weak function of $E(\kappa)$. Variation of the range of integration of (4.1) over ejected-electron momentum led to essential reproduction of the cross-section shape with energy. Although $E(\kappa)$ is a slightly more complicated function of ejected-electron momentum when the band-structure[32] term is included, the actual effect on cross-section determination is small relative to the differences between the Burhop formalism and the measurements. The validity of our ejected-electron-energy approximation is also supported by the experimental cross sections we obtained from different chemical states. For example, no appreciable differences in the measurements were noted for C in the form of ethylene decomposed to yield pure carbon. Measured cross sections varied in magnitude in general agreement with the theory, even though the various adsorbates were in a wide range of chemical states.

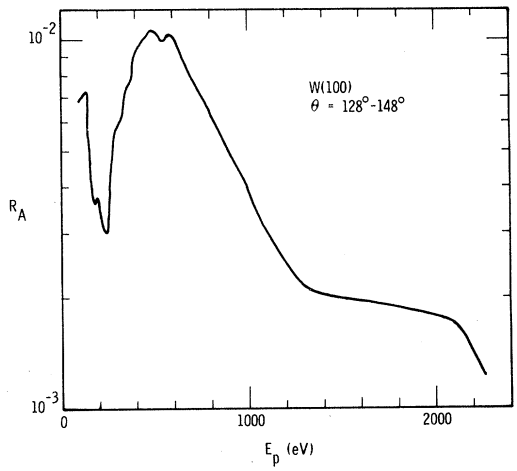

FIG. 8. Measured elastic-scattering coefficient R_A as a function of primary energy.

The measured backscattering cross section for C is shown in Fig. 7 for comparison with the cross sections computed from the Burhop theory for various 20° increments of scattering angle. As noted before, the calculations for 128° to 148° (the experimental analyzer aperture angles) are low. Figure 7 shows that scattering angles of about 50° to 70° give fair agreement in absolute magnitude and slope with the experimental cross sections at $X = 3.0$. This suggests that the effective binary collision scattering angle may be only about 60° for $X \sim 3.0$.

The Coulomb forces of the nucleus on the incident and scattered electrons are neglected in the Burhop theory. These interactions could perhaps distort the incident and scattered waves enough to account for the extra ~80° of scattering. In fact, recent distorted-wave treatments by Shelton, Leherissy, and Madison[33] and by Geltman and Hidalgo[34] of the excitation of the $2s$ hydrogen state show this type of behavior. Plane-wave theories are shown to give far too little scattering in the back direction in comparison with the distorted-wave theory. The divergence between the two theories becomes more pronounced at high energies, just as our data diverge from the plane-wave theory. Due to the similarities between backscattering excitation and ionization, it is likely that a distorted-wave treatment of K-shell ionization will give considerably better agreement with our data.

In conclusion, the data in this paper show that the Burhop ionization theory gives cross sections which are too low, particularly in the high-energy limit, for backscattering ionization of the K shells of C, N, O, Na, and Mg. It is likely that a distorted-wave scattering theory, such as the Coulomb–Born theory, will produce better agreement with experiment for large-angle ionization scattering by K-shell electrons.

APPENDIX: DOUBLE-SCATTERING THEORY

Let the elastic scattering coefficient per unit solid angle for the bare substrate be defined by

$$R(E_p, \hat{k}, \hat{k}') = I_e(E_p, \hat{k}, \hat{k}')/I_0 , \tag{A1}$$

where I_e is the elastic scattering current per unit solid angle for momentum transfer $\hat{k}$ to $\hat{k}'$. The angle between $\hat{k}$ and $\hat{k}'$ is restricted to $\frac{1}{2}\pi$ to π for normal incidence on the sample surface. This elastic-reflection coefficient R is a measurable quantity and thus includes multiple elastic scattering in the substrate. The double-scattering cross section per unit solid angle for total momentum transfer $\hat{k}$ to $\hat{k}''$ is

$$\sigma_{ds}(E_p, \hat{k}, \hat{k}'') = \rho \int_{2\pi} [R(E_p, \hat{k}, \hat{k}')\, \sigma(E_p, \hat{k}', \hat{k}'') + \sigma(E_p, \hat{k}, \hat{k}')\, R(E_p - E_i, \hat{k}', \hat{k}'')]\, d\Omega' , \tag{A2}$$

where ρ is an absorption factor for the overlayer and Ω' is the solid angle for $\hat{k}'$. Multiple elastic scattering within the single atomic overlayer is neglected in (A2) since it is small compared with that of the semi-infinite, heavy-atom substrate. Integration of $\hat{k}''$ over the analyzer aperture solid angle Ω'' obtains the observed double-scattering cross section:

$$\Delta\sigma_{ds}(E_p) = \int_{\text{aperture}} \sigma_{ds}(E_p, \hat{k}, \hat{k}'')\, d\Omega'' . \tag{A3}$$

If σ is strongly peaked in the forward-scattering direction and R is a smooth function of scattering angle, then (A2) and (A3) may be accurately described by

$$\Delta\sigma_{ds}(E_p) = \rho \Delta\sigma_{fs}(E_p)\, [R_A(E_p) + R_A(E_p - E_i)] , \tag{A4}$$

where

$$R_A(E_p) = \int_{\text{aperture}} R(E_p, \hat{k}, \hat{k}'')\, d\Omega''$$

and

$$\Delta\sigma_{fs}(E_p) = \int_F \sigma(E_p, \hat{k}, \hat{k}')\, d\Omega' .$$

The F on the integral means that the integration is performed over angles in the forward-scattering direction where σ is strongly peaked. Equation (A4) was used by us in Ref. 15 with $\rho = 1$ to estimate double scattering. The integration over solid angle Ω' in Ref. 15 was performed for angles of 0° to 20° from the forward direction. That estimate of double scattering is good if σ is sufficiently peaked in the forward-scattering direction and if R is a sufficiently smooth function of the backscattering angle involved, conditions which are obeyed for $X > 2$.

Suppose that σ and R are not functions of scattering angle. Then (A2) and (A3) may be described by

$$\begin{aligned}\Delta\sigma_{ds}(E_p) &= \rho\sigma(E_p)\, [R(E_p) + R(E_p - E_i)] \\ &\quad \times \int_{\text{aperture}} \int_{2\pi} d\Omega'\, d\Omega'' \\ &\approx \rho\, \sigma_T(E_p)\, [R_A(E_p) + R_A(E_p - E)] ,\end{aligned} \tag{A5}$$

where

$$\sigma_T(E_p) = \int_{2\pi} \sigma(E_p, \hat{k}, \hat{k}')\, d\Omega'$$

$$\approx \int_{4\pi} \sigma(E_p, \hat{k}, \hat{k}')\, d\Omega' ,$$

and R_A was previously defined. From Fig. 7 it is seen that σ is roughly constant as a function of scattering angle for small X. In addition, LEED measurements show that R is not a strong function of backscattering angle when averaged over large angles ($\Omega \sim 2\pi$) for 100- to 2000-eV primary energies. Therefore (A5) should be a good estimate of double scattering for small X.

*Work supported by the U. S. Atomic Energy Commission.

[1]J. C. Clark, Phys. Rev. 48, 30 (1935).
[2]A. E. Smick and P. Kirkpatrick, Phys. Rev. 67, 153 (1945).
[3]G. W. Green, in *Proceedings of the Third International Symposium on X-Ray Microscopy, Stanford* (Academic, New York, 1962); thesis (Cambridge University, 1962) (unpublished).
[4]J. W. Motz and R. C. Placious, Phys. Rev. 136, A662 (1964).
[5]H. Hansen, H. Weighmann, and H. Flammersfeld, Nucl. Phys. 58, 241 (1964).
[6]W. Hink and A. Ziegler, Z. Physik 226, 222 (1969).
[7]G. Glupe and W. Mehlhorn, Phys. Letters 25A, 274 (1967).
[8]W. Hink, Z. Physik 177, 424 (1964).
[9]W. Green and V. E. Cosslett, J. Phys. D1, 425 (1968).
[10]W. Hink and H. Paschke, Phys. Rev. A4, 507 (1971).
[11]C. B. O. Mohr and F. H. Nicoll, Proc. Roy. Soc. (London) A138, 229 (1932); A138, 469 (1932); A142, 320 (1933); A142, 647 (1933).
[12]E. H. S. Burhop, Proc. Cambridge Phil. Soc. 36, 43 (1940).
[13]A. M. Arthurs and B. L. Moiseiwitsch, Proc. Roy. Soc. (London) A247, 550 (1958).
[14]H. S. W. Massey and E. H. S. Burhop, *Electronic and Ionic Impact Phenomena* (Oxford U. P., Oxford, 1952), Vol. I, Fig. 81a.
[15]R. L. Gerlach and A. R. DuCharme, Phys. Rev. Letters 27, 290 (1971).
[16]G. A. Harrower, Phys. Rev. 102, 340 (1956).
[17]H. E. Bishop and J. C. Rivière, Appl. Phys. Letters 16, 21 (1970).
[18]R. L. Gerlach, J. Vac. Sci. Technol. 8, 599 (1971).
[19]R. L. Gerlach and D. W. Tipping, Rev. Sci. Instr. 42, 151 (1971).
[20]J. R. Pierce, Bell Tech. J. 24, 305 (1945).
[21]H. Z. Sar-el, Rev. Sci. Instr. 38, 1210 (1967).
[22]H. Hafner, J. A. Simpson, and C. E. Kuyatt, Rev. Sci. Instr. 39, 33 (1968).
[23]P. W. Palmberg, G. K. Bohn, and J. C. Tracy, Appl. Phys. Letters 15, 254 (1969).
[24]R. G. Musket, J. Less Common Metals 22, 175 (1970).
[25]R. L. Gerlach and T. N. Rhodin, Surface Sci. 17, 32 (1969).
[26]K. Siegbahn *et al.*, *ESCA: Atomic, Molecular, and Solid State Structure Studied by Means of Electron Spectroscopy* (Almqvist and Wiksells Boktryckeri, AB, Uppsala, Sweden, 1967).
[27]L. Ramqvist *et al.*, Phys. Chem. Solids 30, 1835 (1969).
[28]H. E. Bishop and J. C. Rivière, AERE Report No. R5834, 1968 (unpublished).
[29]P. J. Estrup and J. Anderson, J. Chem. Phys. 46, 567 (1967).
[30]P. W. Palmberg and T. N. Rhodin, J. Appl. Phys. 39, 2425 (1968).
[31]R. L. Gerlach and A. R. DuCharme, Surf. Sci., (to be published).
[32]L. F. Mattheiss, Phys. Rev. 139, 1893 (1965).
[33]W. N. Shelton, E. S. Leherissey, and D. H. Madison, Phys. Rev. A 3, 242 (1971).
[34]S. Geltman and M. B. Hidalgo, J. Phys. B4, 1299 (1971).